

Efficacy of Hilbert and Wavelet Transforms for Time-Frequency Analysis

T. Kijewski-Correa, A.M.ASCE¹; and A. Kareem, M.ASCE²

Abstract: Two independently emerging time-frequency transformations in Civil Engineering, namely, the wavelet transform and empirical mode decomposition with Hilbert transform (EMD+HT), are discussed in this study. Their application to a variety of nonstationary and nonlinear signals has achieved mixed results, with some comparative studies casting significant doubt on the wavelet's suitability for such analyses. Therefore, this study shall revisit a number of applications of EMD+HT in the published literature, offering a different perspective to these commentaries and highlighting situations where the two approaches perform comparably and others where one offers an advantage. As this study demonstrates, much of the differing performance previously observed is attributable to EMD+HT representing nonlinear characteristics solely through the instantaneous frequency, with the wavelet relying on both this measure and the instantaneous bandwidth. Further, the resolutions utilized by the two approaches present a secondary factor influencing performance.

DOI: 10.1061/(ASCE)0733-9399(2006)132:10(1037)

CE Database subject headings: Spectral analysis; Random waves; Stationary processes; Time series analysis; Frequency analysis; Transformations; Transient loads; Transient response; Nonlinear analysis.

Introduction

The Fourier transform has revolutionized signal processing and its applications to various disciplines, perhaps like no other development, permitting its users to transcend the burdens of time series analysis and view energy content in terms of harmonics. Such merits of Fourier-based analysis have led to its widespread acceptance; however, its inability to handle nonstationary phenomenon has proven problematic. As the Fourier transform decomposes a signal by a linear combination of projections onto an infinite-duration trigonometric basis, it is unable to capture local features, challenging analysts to explore the use of time-frequency transformations, e.g., Gurley and Kareem (1999). While a host of such techniques have surfaced, two approaches have received increased attention: The wavelet transform, e.g., Kareem and Kijewski (2002), and empirical mode decomposition with Hilbert transform (EMD+HT), e.g., Huang et al. (1998). In a number of studies, EMD+HT has been advocated by illustrating its superior performance in comparison to the wavelet transform for a number of examples. However, these results depend greatly on the mode of presentation and the resolutions chosen for the analysis. Therefore, this study will present a

comparison of these two approaches from a different perspective that reconciles each transform's unique characterization of nonlinear and nonstationary information, illustrating cases where the two approaches perform comparably, and highlighting situations where one offers some advantage.

Analytic Signal Theory for Time-Frequency Analysis

The tracking of time-varying frequency content is typically accomplished by monitoring the instantaneous frequency (IF) of the signal, commonly traced back to the notion of a complex analytic signal (Gabor 1946), taking the form of an exponential function given by

$$z(t) = A(t)e^{i\phi(t)} \quad (1)$$

with time-varying amplitude $A(t)$ and phase $\phi(t)$ that is usually generated by

$$z(t) = x(t) + iH[x(t)] \quad (2)$$

where $x(t)$ =real-valued signal being transformed; and the operator $H[\cdot]$ represents the HT given by

$$H[x(t)] = \frac{1}{\pi} P \int_{-\infty}^{\infty} \frac{x(s)}{t-s} ds \quad (3)$$

where s =variable of integration; and P denotes the Cauchy principle value. There are indefinitely many amplitude/phase pairs that can represent an arbitrary real-valued signal; however, the analytic signal as defined in Eq. (1) provides a unique pair given that is generated by a linear operation that suppresses all negative frequencies, e.g., by the HT in Eq. (2). The uniqueness of this representation is guaranteed for *asymptotic signals* or, in other words, signals whose phases vary more rapidly than their amplitudes. This issue will be explored further in Example 5.

From the definition in Eq. (1), Ville (1948) proposed the concept of IF as the time-varying derivative of the phase

¹Rooney Family Assistant Professor, Dept. of Civil Engineering and Geological Sciences, Univ. of Notre Dame, 156 Fitzpatrick Hall, Notre Dame, IN 46556. E-mail: tkijewsk@nd.edu

²Robert M. Moran Professor, Dept. of Civil Engineering and Geological Sciences, Univ. of Notre Dame, 156 Fitzpatrick Hall, Notre Dame, IN 46556. E-mail: kareem@nd.edu

Note. Associate Editor: Nicos Makris. Discussion open until March 1, 2007. Separate discussions must be submitted for individual papers. To extend the closing date by one month, a written request must be filed with the ASCE Managing Editor. The manuscript for this paper was submitted for review and possible publication on July 27, 2004; approved on August 11, 2005. This paper is part of the *Journal of Engineering Mechanics*, Vol. 132, No. 10, October 1, 2006. ©ASCE, ISSN 0733-9399/2006/10-1037-1049/\$25.00.

$$f_i(t) = \frac{1}{2\pi} \frac{d}{dt} \phi(t) = \frac{1}{2\pi} \frac{d}{dt} [\angle z(t)] \quad (4)$$

While the notion of frequency at an instant may seem paradoxical, it may be simply conceptualized as the frequency of a sine wave that locally fits the oscillatory characteristic of the signal under consideration.

Analytic Signals for Multicomponent Signals

While the convolution with $1/t$ in Eq. (3) produces a transform with localized temporal resolution, its Fourier transform yields a sum of Heaviside functions, which lack finite bandwidth—an expected result based on Heisenberg's uncertainty principle. As a result of this ill-defined frequency resolution, the HT cannot distinguish the various frequency contributions of multicomponent signals, requiring such signals to be preprocessed into their monocomponent elements, e.g., by bandpass filtering (Lee and Park 1994), before implementation of the transform. Huang et al. (1998) introduced the concept of EMD as an alternative means to separate multicomponent signals into their monocomponent constituents through a progressive sifting process to yield empirical bases termed intrinsic mode functions (IMFs). These IMFs are defined so as to ensure that they have well-behaved HTs and conform to a narrowband condition. Full details of EMD can be found in Huang et al. (1998). As the stopping conditions on the sifting process are somewhat arbitrary, "infinitely many IMF sets can be generated" (Huang et al. 2003), prompting the development of statistical measures for more definitive stopping criteria. Olhede and Walden (2004) conducted analyses of EMD using various stopping criteria, yet still found oscillatory IF estimates and ill-defined time-frequency spectra with evidence of mode mixing (both of which will also be demonstrated later in this study).

In response to these findings, Olhede and Walden (2004) introduce a discrete wavelet transform/wavelet packet-based decomposition as a replacement for EMD in the preprocessing of multicomponent signals. The authors highlight superior performance of this approach and, by virtue of its nonempirical character, show it to be conducive to statistical analysis for noise reduction. However, unlike Olhede and Walden (2004), in this study, the properties of asymptotic signals, analytic parent wavelets, and the continuous wavelet transform will be utilized as a vehicle to provide a direct approximation to the analytic signal for multicomponent time series, thus eliminating the need for HTs all together.

The continuous wavelet transform is a linear transform that decomposes an arbitrary signal $x(t)$ via basis functions with compact support that are simply dilations and translations of the parent wavelet $g(t)$

$$W(a, t) = \frac{1}{\sqrt{a}} \int_{-\infty}^{\infty} x(\tau) g^* \left(\frac{t - \tau}{a} \right) d\tau \quad (5)$$

where $*$ denotes the complex conjugate (Mallat 1998). Dilation by the scale, a , inversely proportional to frequency, allows the various harmonic components of the signal to be captured. The wavelet coefficients, $W(a, t)$, provide a measure of the similitude between the dilated/shifted parent wavelet and the signal at time t and scale a . The squared magnitude of the coefficients in Eq. (5) can be presented via the scalogram as energy content in frequency and time, as shown in Fig. 1 through a three-dimensional and two-dimensional perspective for a quadratic chirp. It should be

noted that there are countless parent wavelets used in practice, with properties that offer distinct benefits depending on the signal characteristics being sought. However, the heavy dependence of results upon the parent wavelet chosen may have motivated the development of EMD to yield a basis derived from the data itself, ensuring that the decomposition would retain some physical resemblance to the original time series. As observed by Olhede and Walden (2004), EMD's independence potentially offers both "a strength (adaptivity) and a weakness (resistance to statistical analysis)."

For analyses seeking to underscore the harmonic character of nonstationary and nonlinear signals, the Morlet wavelet is often adopted (Grossman and Morlet 1985)

$$g(t) = e^{-t^2/2} e^{i2\pi f_o t} = e^{-t^2/2} (\cos(2\pi f_o t) + i \sin(2\pi f_o t)) \quad (6)$$

which possesses a unique relationship between the scale a and the Fourier frequency f at which the wavelet is focused: $a = f_o / f$, where $f_o = \text{central frequency}$.

Wavelets, such as those in Eq. (6), have a tendency to concentrate their largest coefficients at the dominant frequency components of the signal and are analytic in form, suppressing negative frequencies much like the HT. Thus, a slice of the wavelet scalogram at a given time produces an instantaneous spectrum (Fig. 1), which peaks at the IF of the signal with measurable spread associated with the instantaneous bandwidth of the signal (Kijewski-Correa 2003). This concentration of energy forms definitive *ridges* or stationary points, as shown schematically in Fig. 1, from which the wavelet IF can be directly identified (Mallat 1998)

$$a_r(t) = \frac{\omega_o}{\phi'(t)} = \frac{f_o}{f_i(t)} \quad (7)$$

It has been shown in Carmona et al. (1998) that, as a signal more strictly meets the asymptotic signal assumption, i.e., as the oscillations of the phase term increase relative to the amplitude term, the better the wavelet coefficients in the vicinity of the stationary points approximate the analytic signal: $W[a_r(t), t] \propto z(t)$. This finding then allows the wavelet coefficients at these stationary points, termed the *wavelet skeleton*, to be directly used to estimate the analytic signal in Eq. (1), instead of the HT in Eq. (2). An example of the resulting real and quadrature-shifted imaginary component of the signal is presented in Fig. 1. Thus, the IF can be identified from the scales in Eq. (7) to form a wavelet IF spectrum (WIFS) (Kijewski-Correa 2003). As shown in Fig. 1, this yields a crisp point estimate comparable to that produced by EMD+HT. Further, the wavelet's phase can also be used in Eq. (4) to more precisely determine the IF. However, Feldman and Braun (1995) noted that the estimate of the IF from phase information may be high in variance, and concluded that a lower variance estimate may be obtained directly from the maxima of time-frequency distributions, as shown in Eq. (7); a fact previously confirmed by Boashash (1992a). This dual characteristic of the wavelet transform, allowing identification of IF by Eq. (7) or Eq. (4), provides alternatives that can be exploited depending upon the situation, whereas the HT relies entirely on phase information for its IF estimates.

Finally, as the wavelet is a transform in both frequency and time, it can implicitly handle multicomponent signals, identifying each component by a distinct ridge in the time-frequency plane. These ridges can be extracted by a variety of techniques (Carmona et al. 1998), though, for the purposes of this study, the basic detection technique associated with the local maxima of the scalogram is invoked.

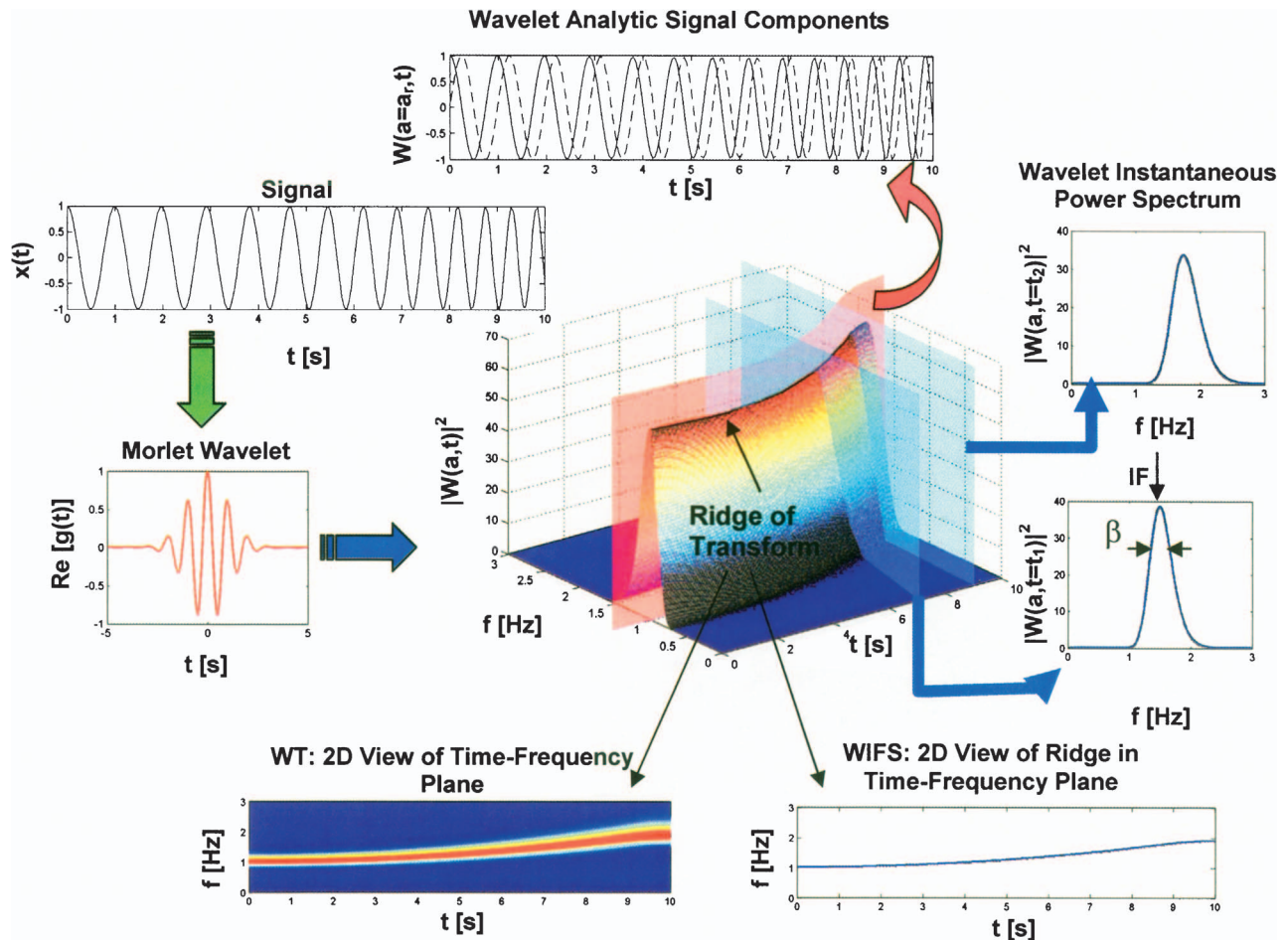


Fig. 1. (Color) Schematic of various wavelet representations for quadratic chirp

Examples

The following sections shall revisit a number of examples presented originally in Huang et al. (1998), examining the authors' EMD+HT results against revised Morlet wavelet results. These revised findings are generated through a framework discussed in Kijewski and Kareem (2003), which addresses issues such as the discretization of the time-frequency plane and corrections for end effects. During this process, it is also necessary to tailor the resolutions of the wavelet transform to extract relevant time or frequency details through the adjustment of the central frequency in Eq. (6) (Kijewski and Kareem 2003). The time and frequency resolutions associated with the frequency f_i for a given central frequency are, respectively, described by $\Delta t_i = f_o / (f_i \sqrt{2})$ and $\Delta f_i = f_i / (2\pi f_o \sqrt{2})$. As such, the dilated Morlet wavelet—centered at time t_i and frequency f_i —symmetrically windows a portion of the signal $2\Delta t$ wide in the time domain, and consequently analyzes a $2\Delta f$ window in the frequency domain to form a Heisenberg box.

Since EMD+HT actually displays IF as a function of time, it is not appropriate to make comparisons solely to wavelet scalograms, which merely depict the time-frequency energy distribution (Fig. 1). Thus wavelet estimates of IF, displayed in the WIFS (Fig. 1), will provide the elementary basis for comparison with EMD+HT results. Any additional HT analyses, beyond those provided in Huang et al. (1998), are generated using the HT as defined in MATLAB, while the differentiation in Eq. (4) was accomplished by determining the slope of a least-squares fit to

the phase data. For reference, the original wavelet analyses conducted by Huang et al. (1998) are also provided, though specific details on the central frequency employed were not reported by the authors.

Example 1: Localized Sine Wave

The first example presented is a single cycle of a 1 Hz sine wave. Figs. 2(a and b) display the signal and the scalogram generated using the Morlet wavelet with localized temporal resolution ($f_o = 1$ Hz). The dark patch in the center of the wavelet map indicates the time-frequency energy concentration of the signal, though in a contoured representation. However, the WIFS in Fig. 2(c) more precisely identifies the IF of the signal as 0.98 Hz from 4.1–4.2 and 4.8–4.9 s, and as 1.0 Hz between 4.3 and 4.7 s, in comparison to Huang et al.'s (1998) wavelet result [Fig. 2(d)]. Though it was previously argued that wavelets require spurious harmonics to represent the transient (Huang et al. 1998), viewing the WIFS affirms that the resolution capabilities of the wavelet analysis are comparable to the EMD+HT analysis [Fig. 2(e)], and may even surpass its performance at the initiation and termination of this single oscillation.

Example 2: Sine Wave with Frequency Discontinuity

Another example of a sudden change in frequency content is provided by a 0.03 Hz sine wave that suddenly shifts to a 0.015 Hz frequency of oscillation at the 500th s, as shown in Fig. 3(a).

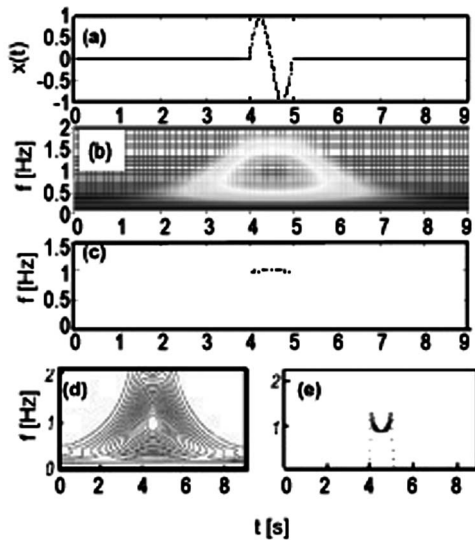


Fig. 2. Example 1: (a) Isolated cycle of 1 Hz sine wave; (b) scalogram; (c) WIFS; (d) original Morlet wavelet result [adapted from Huang et al. (1998)]; (e) EMD+HT result [adapted from Huang et al. (1998)]

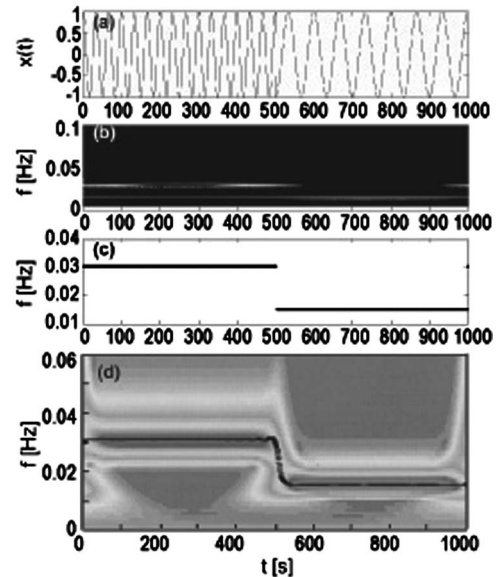


Fig. 3. Example 2: (a) Cosine wave with frequency halved midway through signal; (b) scalogram; (c) WIFS; (d) original Morlet wavelet result with HT+EMD result superimposed [adapted from Huang et al. (1998)]

The initial wavelet analysis by Huang et al. (1998) indicates a smearing of energy in both frequency and time, and pales in comparison to the pinpoint precision of the EMD+HT result, as shown in Fig. 3(d). Revisiting this example, but refining the frequency resolution properties of the Morlet wavelet ($f_o=5$ Hz), two distinct frequency bands are identified in Fig. 3(b), although the point of transition is obscured in the scalogram representation. However, upon examining the WIFS in Fig. 3(c), the precision of the wavelet IF estimation is evident.

Example 3: Quadratic Chirp

While the ability of both approaches to detect sudden changes in frequency has thus far been demonstrated, their ability to capture a continuous change in frequency is now demonstrated via HTs and continuous wavelet ($f_o=3$ Hz) transforms of the quadratic chirp shown in Fig. 4(a). Note that the analysis of this chirp signal does not require preprocessing by EMD, as it possesses a unique frequency component at each instant in time. The Hilbert and wavelet IF estimates are shown in Fig. 4(b). The HT result manifests an unexpected oscillation, in addition to the global quadratic decay. The wavelet transform does not depict this oscillatory behavior, but instead results in a piece-wise fit to the changes in frequency that nearly identically overlaps the actual IF law. This piece-wise fit arises from the fact that the wavelet fits small waves or “wavelets” to the signal at each point in time—as expected, a locally linear approximation to the quadratic.

Example 4: Linear Sum of Two Closely-Spaced Cosines

The following example will demonstrate a situation in which the frequency resolution capabilities of EMD can be problematic. Consider a pair of closely spaced cosine waves given by

$$x(t) = \cos\left(\frac{2}{30}\pi t\right) + \cos\left(\frac{2}{34}\pi t\right) \quad (8)$$

The frequencies of these two harmonics are approximately 0.0294 and 0.0333 Hz. Fig. 5(a) shows the signal with characteristic beat phenomena. In order to separate the two components, a given analysis technique must have a refined frequency resolution, consistent with the findings of Delprat et al. (1992). In Huang et al. (1998), it was shown that neither a continuous wavelet analysis nor EMD+HT could identify two distinct harmonic components. Revisiting this problem using a wavelet with $f_o=5$ Hz, two IF components can be identified at 0.0303 Hz and 0.0340 Hz, within 3% of the actual signal frequencies, as shown by the WIFS in Fig. 5(b). Fig. 5(c) displays the wavelet scalogram obtained by Huang et al. (1998) with the EMD+HT result superimposed as contours. Though the signal is the linear combination of two distinct harmonics, neither result in Fig. 5(c) accurately reflects this. However, the continuous wavelet’s inability to separate the harmonics in Huang et al. (1998) should not be interpreted as a failure of the continuous wavelet in theory, but rather a byproduct of the selection of an insufficient central frequency f_o in the analysis.

Note that the EMD+HT result in Fig. 5(c) localizes in the same vicinity, but also shows some spurious oscillatory behavior in the IF between 0.025 Hz and 0.035 Hz, treating the pair of harmonics as a frequency-modulation (FM) wave. The presence of multiple components in an IMF will result in nonlinear phase terms once the HT is applied. In such cases, the HT treats the closely spaced harmonics as an FM wave. The misrepresentation in this example may be a direct consequence of EMD’s inadequate frequency resolution. In this case of two closely spaced modes, the EMD required a very stringent condition of 3,000 siftings to obtain only eight IMFs, which still could not represent the true signal (Huang et al. 1998). The inability to distinguish between two distinct components may be traced to the narrowband conditions invoked in the extraction of IMFs. The use of a more relaxed narrowband condition, placing restrictions on the

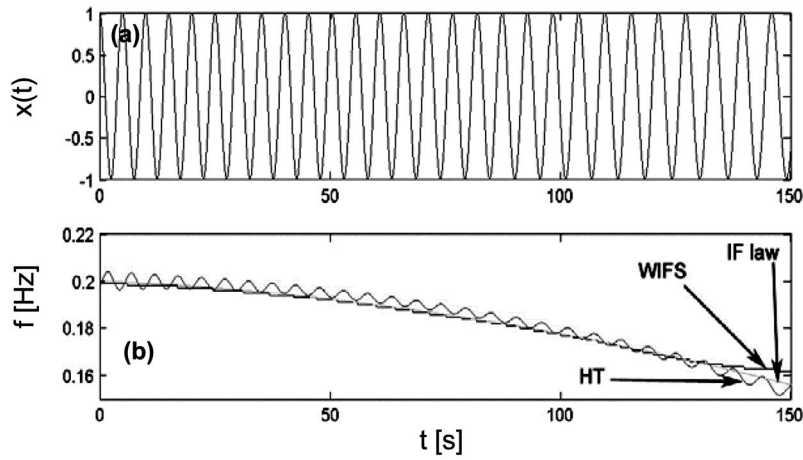


Fig. 4. Example 3: (a) Quadratic chirp; (b) identified IF by wavelet transform and HT with actual IF law

number of zero crossings and maxima, may yield IMFs that are narrowband in character but not strictly monocomponent, potentially encapsulating in that narrow band both closely spaced harmonics. This was demonstrated by Wu and Huang (2004), where the authors effectively establish EMD as a dyadic filter, and IMFs are shown to concentrate their Fourier spectrum at distinct frequencies but with considerable overlap in bandwidth. Thus, the EMD is ill-equipped to capture the dual harmonic character of signals with closely spaced frequency components, instead treating it as some non-physical FM wave. In an extensive evaluation of EMD+HT performance, restrictions, and limitations in characterizing irregular water waves, Dätig and Schlurmann (2004) categorically stated EMD's inability to separate harmonic components that have frequency proportions near unity. The authors consider this to be one of the primary limitations of EMD, which surfaced in their parametric study of waves, when some higher-order nonlinear components close in frequency were not distinctly identified. Rather, these are added on to the fundamental riding wave. Similar findings were also noted by Olhede and Walden (2004), where EMD's poor frequency resolution allowed mode mixing in combinations of sine waves, yielding leakage in the EMD projection. However, it should be noted that Huang et al. (2003) recently attempted to address the issues of mode mixing in IMFs through a confidence limit-based approach. Despite this, the empirical nature of EMD still presents some difficulty in quantifying and refining frequency resolutions.

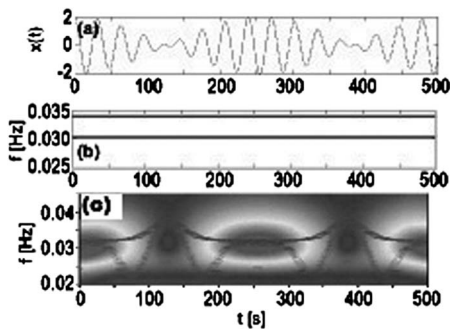


Fig. 5. Example 4: (a) Cosine pair; (b) WIFS; (c) original wavelet and superimposed EMD+HT results [adapted from Huang et al. (1998)]

Example 5: Amplitude Modulated Cosine with Constant Frequency

In the following example, the issue of physical significance versus mathematical anomaly is again explored. Consider an amplitude-modulated wave generated by

$$x = \exp(-0.01t)\cos(2\pi f_n t) \quad (9)$$

where $f_n = 0.0313$ Hz. This parallels the impulse response function of a single-degree-of-freedom mechanical oscillator with damping of approximately 5% critical, shown in Fig. 6(a). Although the signal is completely amplitude modulated in theory, there is a minor frequency modulation revealed upon applying the

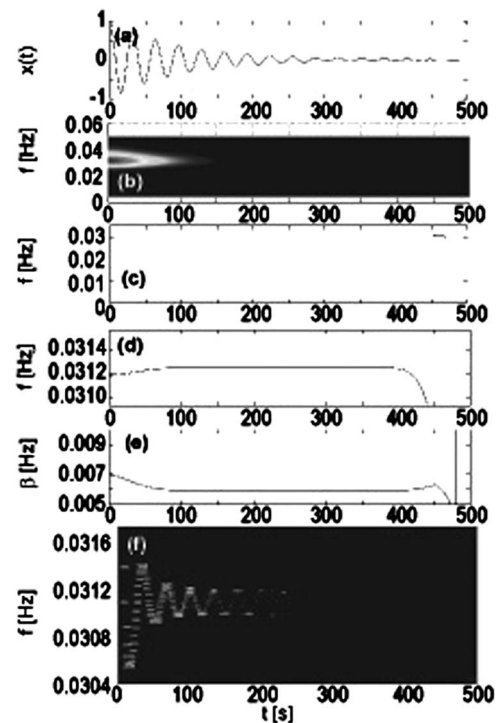


Fig. 6. Example 5: (a) Amplitude-modulated cosine; (b) scalogram; (c) WIFS; (d) IF by wavelet phase; (e) wavelet instantaneous bandwidth; (f) EMD+HT result [adapted from Huang et al. (1998)]

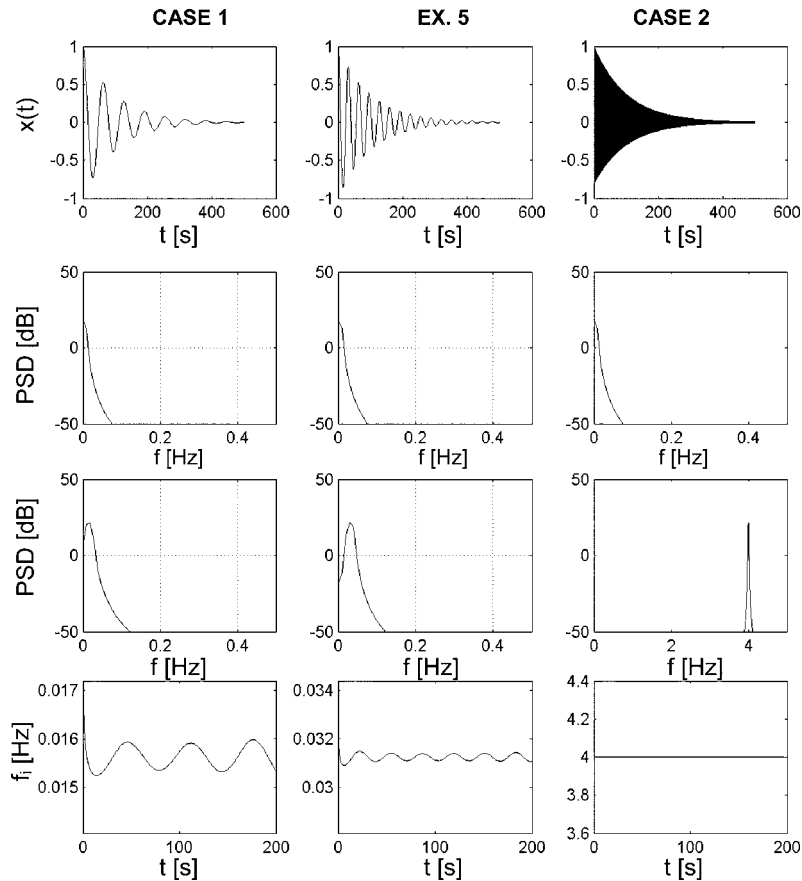


Fig. 7. Results matrix: Simulated signal (row 1), amplitude PSD (row 2), phase PSD (row 3), and $f_i(t)$ by HT (row 4)

HT, as shown in Fig. 6(f). Huang et al. (1998) argued that this result should be expected as amplitude variations influence the bandwidth of a process, viewed in terms of traditional power spectra as a spread of frequencies about the mean frequency. Based on that argument, the authors contend that this spread of frequency may be manifested in time as a slight deviation of the IF from the mean frequency of the process, in this case yielding oscillations about a frequency of 0.0313 Hz. This spread of frequencies about the IF, at each instant in time, is one means to account for the many neighboring frequencies produced by amplitude modulation, however, the IF should theoretically surface as the average of the frequencies at each point in time, as discussed in Priestley (1988), and would not be expected to oscillate for this linear system. As the signal has no true FM, how should the oscillatory component detected by the HT be interpreted?

On the other hand, the analysis by the continuous wavelet transform ($f_o=1$ Hz), shown in Fig. 6(b), captures the transient nature of the signal with the energy content concentrated near 0.03 Hz. The WIFS [Fig. 6(c)] identifies a constant frequency value of 0.0315 Hz. As the wavelet phase often can be a more precise means of identifying the IF, it is a useful exercise to see if the wavelet can detect any physical influence of amplitude modulation through this measure. As shown in Fig. 6(d), the wavelet phase takes on a constant value of 0.0313 Hz and—when zoomed in to a scale of $\pm 1\%$ of the oscillator frequency—there is no evidence of oscillation. There is a slight deviation early in the signal, corresponding to a residual byproduct of end effects. At the end of the signal, the estimation quality rapidly degrades due to the difficulty of phase identification once the signal energy is nearly completely damped out.

However, the spectral characteristics of a system are not merely defined by the IF, which will always surface as the average of the frequencies at each point in time (Priestley 1988). The spread of frequencies contributing to this average measure is also of interest, as described by the bandwidth (β) of the instantaneous wavelet spectra (Kijewski and Kareem 2002). For single-degree-of-freedom oscillators like the one considered here, the bandwidth has a unique relationship with the oscillator frequency and its damping. The bandwidth of each instantaneous spectrum produced from the wavelet analysis is provided in Fig. 6(e), which demonstrates that this value holds relatively constant throughout the decay in the signal; as expected, since the expression in Eq. (9) represents an oscillator with a constant frequency and damping. Note that at the beginning of the signal, the bandwidth suffers from a more visible inaccuracy, attributed to the fact that the bandwidth measure is far more sensitive than the IF to end effects, as discussed in Kijewski and Kareem (2002, 2003). Even with the addition of padding, bandwidth measures within $3\Delta t$ of the beginning and end of the signal can have some residual inaccuracy, clearly marked by the rounded characteristic in Fig. 6(e). Neglecting these two regions, the bandwidth holds constant, as expected.

Contrary to the EMD+HT result, oscillatory FMs are not reflected in the wavelet bandwidth measure or in the IF identified using either the ridge scales or phase of the wavelet analytic signal representation. In fact, the presence of amplitude modulations in this signal is ultimately observed in the amplitude of the wavelet skeleton, which reflects the decay of energy in the signal. This information has been used in system identification applications, where nonlinearities in damping and stiffness are,

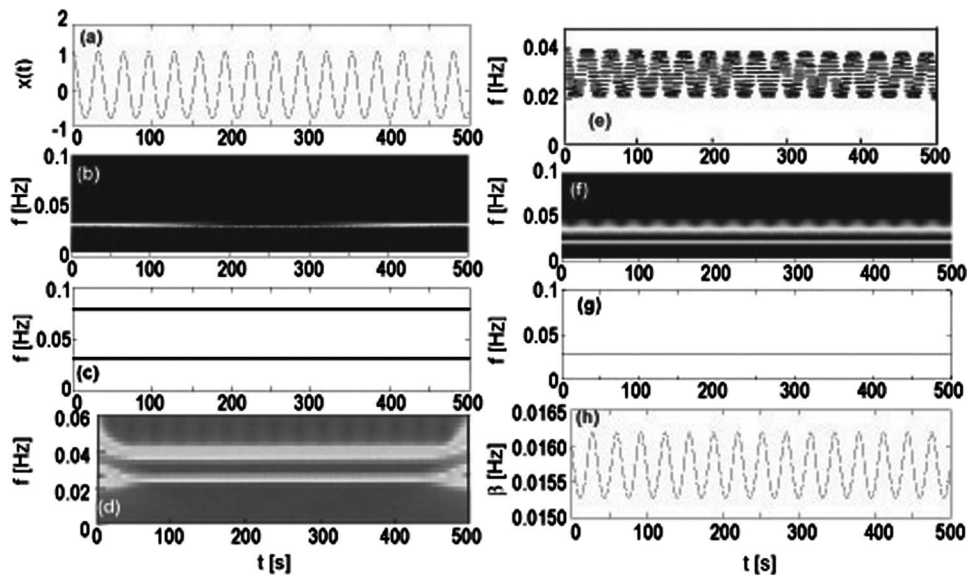


Fig. 8. Example 6: (a) Second-order approximation to the Stokes wave; (b) scalogram ($f_o=5$ Hz); (c) WIFS ($f_o=5$ Hz); (d) original Morlet wavelet result [adapted from Huang et al. (1998)]; (e) EMD+HT result [adapted from Huang et al. (1998)]; (f) scalogram ($f_o=0.5$ Hz); (g) WIFS ($f_o=0.5$ Hz); (h) wavelet instantaneous bandwidth ($f_o=0.5$ Hz)

respectively, detected via changes in the wavelet amplitude and phase (Feldman 1994; Staszewski 1998; Kijewski and Kareem 2003). Thus, while the notion of intrawave FM may be physically meaningful in some cases, in this example, the presence of this phenomenon is not, indicating a slight nonlinearity in a linear system.

While the analytic signal generated using the HT will always provide a unique complex representation, as Boashash (1992b) stated, “whether or not it corresponds to any physical reality is another question.” This indeed depends on the extent to which asymptotic signal assumptions are met. In this example, the presence of FM in a constant frequency oscillator can be deceiving, and may actually be the consequence of a violation of asymptotic signal assumptions. The definition of the IF in Eq. (4) is only valid when the Fourier transform of $A(t)$, in the complex analytic signal in Eq. (1), is well separated from and less than the Fourier transform of $\exp[i\phi(t)]$. This is because the HT inherently selects the highest-frequency component of the signal as the complex phase term. If the Fourier spectrum of the phase component of the signal is not located at a frequency higher than—and well separated from—the amplitude spectrum, then the HT operation will be a result of overlapping and phase-distorted functions. This will give rise to a waveform that can no longer be described by a purely amplitude-modulated law, even though it was generated by an amplitude-modulated process (Rihaczek 1966). In such cases, “the Hilbert transform and the analytic signal are not always interpretable in a way which is physically meaningful and representative of physical phenomena” (Boashash 1992b). Such manifestations were noted by Olhede and Walden (2004) to be the result of “leakage-generated oscillations” in the EMD+HT result.

To explore the importance of separation between amplitude and phase components, three real components of an analytic signal, having the form of Eq. (9), are generated: The original example of $f_n=1/32$ Hz (Example 5), $f_n=1/64$ Hz (Case 1), and $f_n=4$ Hz (Case 2). For each of these cases, the power spectral density (PSD) of the amplitude term and of the phase term are presented in the results matrix in Fig. 7. From this figure, one can see that Case 1 provides the most significant overlap of spectral

energy between amplitude and phase; Case 2 provides the least. The IFs identified by the HT are provided in the fourth row of the results matrix (Fig. 7). The y axes on these figures are scaled to $\pm 10\%$ of f_n for each case, to provide an equivalent basis for comparison. In the case where the overlap is most significant (Case 1), the level of “intrawave modulation” is most marked. As the overlap is lessened, the intrawave modulation is still present but reduced (Example 7). In both of these cases, the periodicity of the oscillations is consistent with f_n used in the simulation. For Case 2, evidence of oscillations is hardly visible. For quantitative purposes, let the IF oscillation factor be defined as the standard deviation of $f_i(t)$ normalized by f_n . The following results are then obtained based on Fig. 7: The oscillation factor for Case 1 is 1.45%, 0.43% for Example 5, and $4.7 \times 10^{-4}\%$ for Case 2. These findings clearly indicate that the magnitude of these modulations significantly depends on the separation between the amplitude and phase in the Fourier domain. It can be inferred that the intrawave modulation, at least in this example, actually results from the HT not being able to clearly identify the phase and misinterpreting contributions from the envelope as a result of their overlap in the Fourier domain, violating asymptotic signal assumptions.

In the case of this exponentially decaying envelope, by increasing the frequency of the oscillatory term in Eq. (9), the degree of overlap is minimized, and the bandwidth of the system is increased. It has been shown that the IF is difficult to accurately identify for signals with a short duration and small bandwidth (Boashash 1992b). Thus, the demonstrations in Fig. 7 further illustrate that oscillations in IF diminish as the signal bandwidth increases. Both the spectral overlap between the phase and amplitude and bandwidth implications serve as viable explanations for the apparent “intrawave” modulation in Fig. 7, and demonstrate that this characteristic is not a physical, but a numerical, byproduct of the HT.

Example 6: Stokes Wave

The implications of central frequency tailoring of wavelet-based analyses are further explored in the example of the idealized

Stokes wave in deep water. The use of a perturbation analysis to solve this system illustrates the common practice of representing nonlinear phenomena as a summation of harmonic components, with the second-order approximation to the Stokes wave profile given by

$$x(t) = \frac{1}{2}\alpha^2 k + \alpha \cos(\omega_s t) + \frac{1}{2}\alpha^2 k \cos(2\omega_s t) \quad (10)$$

where α =amplitude; and k =wave number. Fig. 8(a) is generated by choosing $\alpha=1$, $k=0.2$, and $\omega_s=2\pi/32$, as discussed in Huang et al. (1998). Fig. 8(b) displays the resulting Morlet wavelet ($f_o=5$ Hz) scalogram, whose color scales do not clearly reflect the second mode, similar to the finding by Huang et al. (1998) in Fig. 8(d). Note, however, that the WIFS in Fig. 8(c) does detect the two harmonics. This Morlet wavelet analysis—though having a refined frequency resolution—has poor temporal resolution, and thus approaches the infinite basis of the Fourier transform and the representation in Eq. (10): approximating the nonlinear Stokes wave as a sum of two harmonics. It has no ability to capture the local nonlinearities of the wave profile.

In contrast, Fig. 8(e) displays the EMD+HT result, which oscillates about 0.0313 Hz and shows no evidence of the second mode. This representation, as discussed in Huang et al. (1998), is consistent with the modeling of the Stokes wave as a FM signal

$$x(t) = \cos[\omega_s t + \varepsilon \sin(\omega_s t)] \quad (11)$$

A visual inspection of the simulated Stokes wave in Fig. 8(a) demonstrates that there is a subtle departure from the simple sinusoidal shape, indicative of FM, represented by the second term in Eq. (11). This can be viewed as a system with *subcyclic* frequency modulation, i.e., changes in frequency that occur within one cycle of oscillation, or in the terminology of Huang et al. (1998), *intra-wave* FM. This is held in contrast to the concept of *supercyclic* oscillations that occur over the course of one or more cycles or due to rapid changes in amplitude.

Interestingly, the wavelet transform can also be tailored to achieve this result. A second wavelet analysis ($f_o=0.5$ Hz) of the Stokian wave simulated by Eq. (10) is also provided in Fig. 8. The scalogram [Fig. 8(f)] still concentrates near 0.03 Hz; however now without evidence of a higher harmonic. Instead there is an oscillatory variation toward the high-frequency range, shown by the lighter hues extending toward 0.1 Hz. An inspection of the WIFS [Fig. 8(g)] still does not confirm this, as it manifests a single constant frequency component at 0.0303 Hz. It was discussed in Example 5 that the instantaneous bandwidth can be used to monitor deviations from the IF or mean frequency, resulting from nonlinearity or physically meaningful intrawave FMs. The instantaneous bandwidth of the wavelet spectra is provided in Fig. 8(h), and demonstrates that this value oscillates with a period of approximately 32 s in the same manner as the EMD+HT result in Fig. 8(e).

The application of a similar wavelet analysis on measured surface elevation data from a wave tank verifies these characteristics of Stokian waves. Fig. 9(a) displays wave data mechanically generated by a 1 Hz sinusoidal excitation with ± 9 mm amplitude. Note that the time series manifests narrowed peaks and widened troughs, highlighting the nonlinear signature. The wavelet analysis ($f_o=0.5$ Hz) produces a scalogram in Fig. 9(b), concentrating near 1 Hz, but with energy fluctuating in the higher frequencies—again indicating the presence of time-varying frequency content. The WIFS in Fig. 9(c), as observed in the previous example of Stokian waves, remains constant at 0.94 Hz, giving an averaged

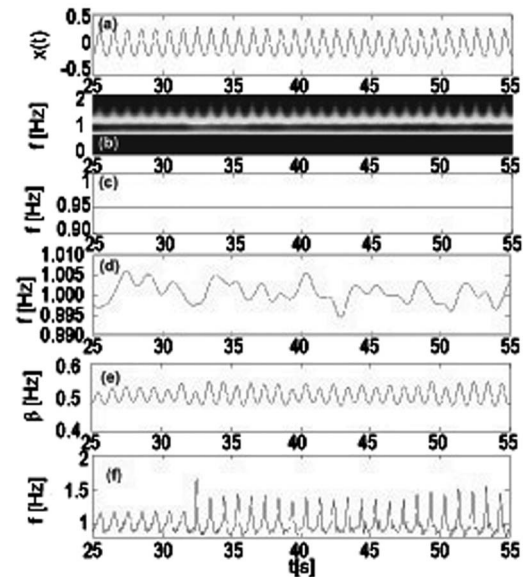


Fig. 9. (a) 30 s of wave tank surface elevation; (b) scalogram; (c) WIFS; (d) IF from wavelet phase; (e) wavelet instantaneous bandwidth; and (f) IF from HT phase

interpretation of the IF. Zooming in on the more precise phase-based IF estimate, in Fig. 9(d), minor modulations reveal time variance in the local mean frequency. Further fluctuations about this mean frequency are then identified in the instantaneous bandwidth in Fig. 9(e), which provides a rich display of nonlinear characteristics beyond that of the numerically simulated Stokes waves in Fig. 8. The bandwidth in this case oscillates—again about the frequency identified in the WIFS; however, the modulations of the bandwidth indicate the periodicity of frequencies concomitant at each instant in the signal. An EMD+HT analysis by Huang et al. (1998) of measured wave data affirmed similar phenomena, albeit displayed solely in the IF. The direct application of the HT in Fig. 9(f) can also affirm the variations of the frequencies present in the system, though this perspective is potentially noisier without the benefit of filtering afforded by EMD.

This example illustrates two important facts. First, a wavelet analysis with poor temporal resolution inherently treats the signal in the same manner as Fourier analysis, while a wavelet analysis with refined temporal resolution is capable of detecting nonlinear wave characteristics. Thus, it is the resolution—tied to a specific analysis—that ultimately dictates whether the nonlinear system will be represented by a series of harmonics as in Eq. (10) or by intrawave modulated waves as in Eq. (11). Second, but perhaps a more important distinction, the wavelet does not necessarily manifest these indicators in the IF, but instead in tandem with the instantaneous bandwidth. Recall again that the wavelet fits small waves, or “wavelets,” to the signal at each point in time. In the case of the Morlet wavelet, these localized waves are sinusoidal in nature. The IF is then the frequency of the best-fit widowed sinusoid. However, as the Stokian wave profile subtly deviates from the simple sinusoid, it is not unreasonable to expect that additional neighboring frequencies are required to capture these deviations through a “localized harmonic series” quantified by the instantaneous bandwidth measure. Thus, the wavelet IF is the mean frequency, and the bandwidth reflects the deviation of these frequencies from this mean as they evolve in time (Priestly 1988). Apparently, these nuances have been overlooked by other recent

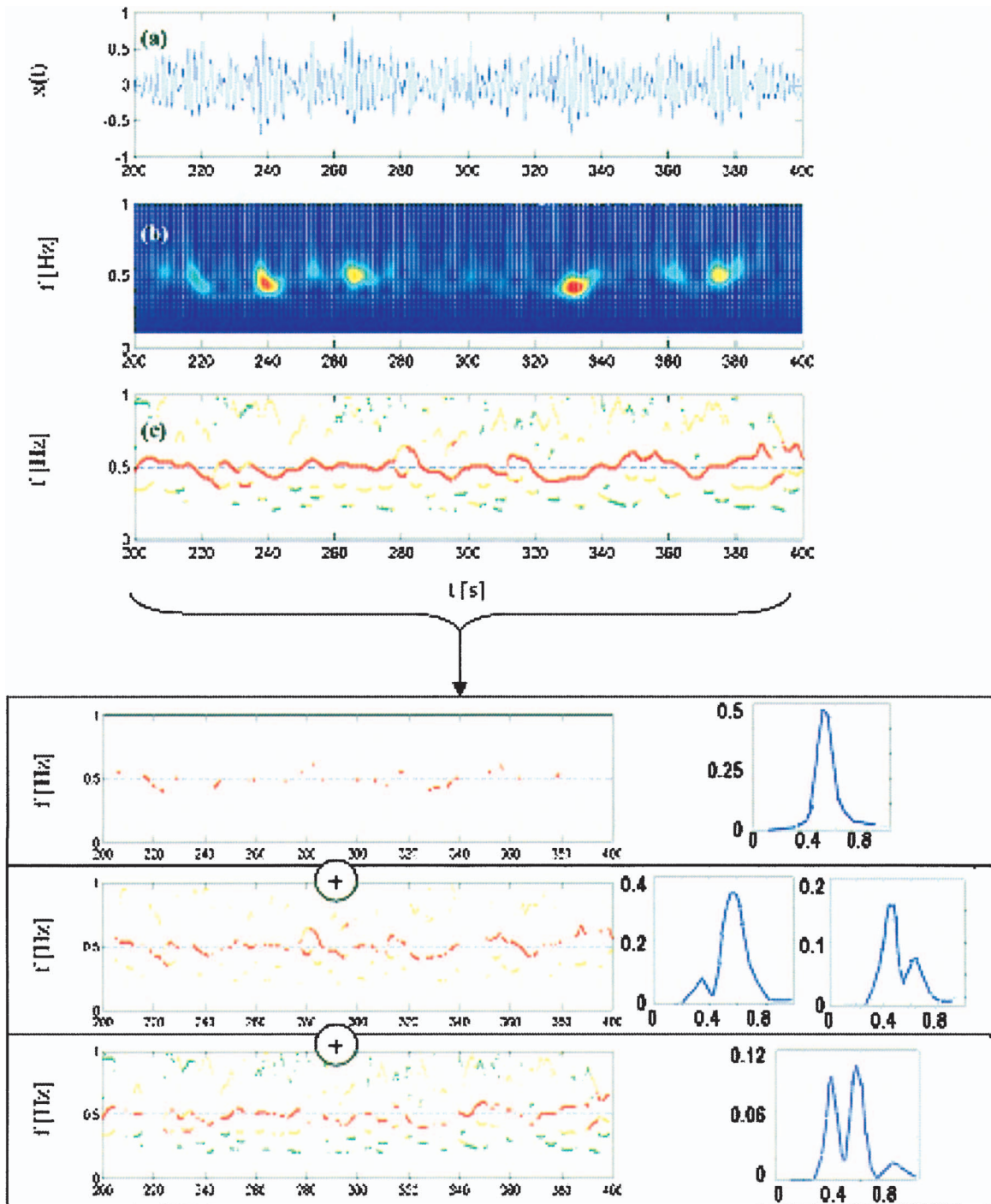


Fig. 10. (Color) Example 7: (a) Measured random wave data; (b) scalogram; (c) WIFS with three primary components (dark \rightarrow light indicates highest- to lowest-energy contributions at each time step) with constitutive ridge elements from unimodal; bimodal, and multimodal response and example of each instantaneous spectral class

studies. For example, Schlurmann (2002) investigated a “monochromatic wave” by EMD+HT and Morlet wavelet transform, though using a fixed central frequency. By solely investigating the wavelet scalogram, without the benefit of an IF or bandwidth estimate, the author found what appears to be a single constant harmonic representing the nonlinear wave, and concluded that this misrepresentation is “due to the uncertainty principle of this [wavelet] technique” (Schlurmann 2002). This demonstrates a common misunderstanding of how wavelet transforms characterize subcyclic nonlinearities, leading in turn to erroneous

conclusions, particularly since no transformation can completely escape the constraints of the uncertainty principle, both EMD+HT, and the wavelet transform alike.

Example 7: Measured Wave Data

To further explore wavelet capabilities for the analysis of waves, the example of experimentally observed random sea waves is presented herein. The waves were generated by a JOint North Sea Wave Project (JONSWAP) spectrum with amplitude of 64 cm.

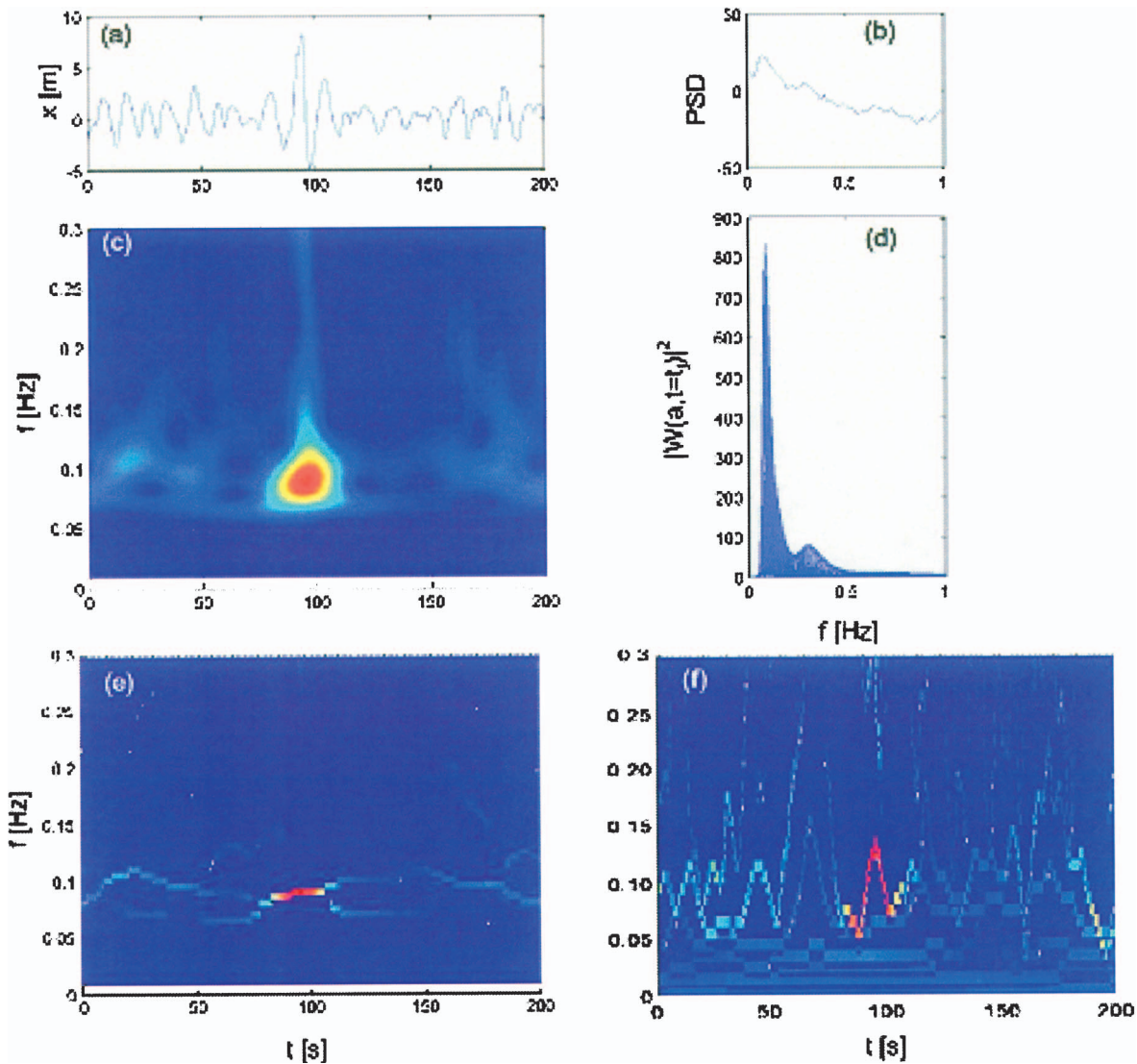


Fig. 11. (Color) (a) Measured transient wave; (b) Fourier power spectrum; (c) wavelet scalogram; (d) superposition of wavelet instantaneous power spectra; (e) WIFS; and (f) EMD+HT result

The signal contains energy over a range of frequencies up to 2 Hz, with a dominant wave frequency of approximately 0.4 Hz. A 200 s sample of the resulting waves at one measuring station is provided in Fig. 10(a). A continuous wavelet analysis with $f_o=1$ Hz yields the scalogram shown in Fig. 10(b). The scalogram reflects several pockets of intense energy bursts, associated with high amplitude events in the data and concentrates around 0.5 Hz. The presence of lighter hues fading into the high-frequency range again suggests a distribution of energy beyond the dominant wave frequency. Ridge extraction from the wavelet modulus revealed up to three local maxima at any given instant, generally concentrating the most energy in the vicinity of 0.5 Hz, as shown by the WIFS in Fig. 10(c). This is accompanied by intermittent lower amplitude components at adjacent frequencies. By breaking the WIFS into its constitutive elements, three modes of response are observed: Unimodal at 0.5 Hz, alternating bimodal at 0.4 and 0.6 Hz, and multimodal. The multimode case can be viewed as a special case of the bimodal response with an intermittent third peak of relatively low energy. It is important to reiterate that wavelet instantaneous spectra, when viewed in tandem with the WIFS, serve as a microscope for studying the evolution of

multiple harmonic components within the response. In particular, the alternating characteristic of the bimodal response represents a temporal variation of the fundamental wave frequency that would be obscured in traditional Fourier analysis. This observation, coupled with the intermittent characteristics, further highlights the richness of the energy distribution in the wave profile.

To further the discussion on the classification of waves by time-frequency analysis techniques, consider the case of a transient “freak wave” measured off the coast of Yura in the Sea of Japan (Schlurmann 2002). The freak wave results from the coalescing of several wave components as a result of a shift in phase. This wave, shown in Fig. 11(a), was analyzed by Schlurmann (2002) using continuous Morlet wavelets and EMD+HT. As shown by the Fourier power spectrum in Fig. 11(b), the wave is dominated by a carrier wave near 0.1 Hz, though with a larger bandwidth that suggests modulation by neighboring frequencies; yet the intermittency of these wave components cannot be portrayed. To faithfully characterize the transient event, a time-frequency approach is required. The continuous wavelet scalogram ($f_o=1$ Hz) is provided in Fig. 11(c), which verifies the concentration of energy near 100 s

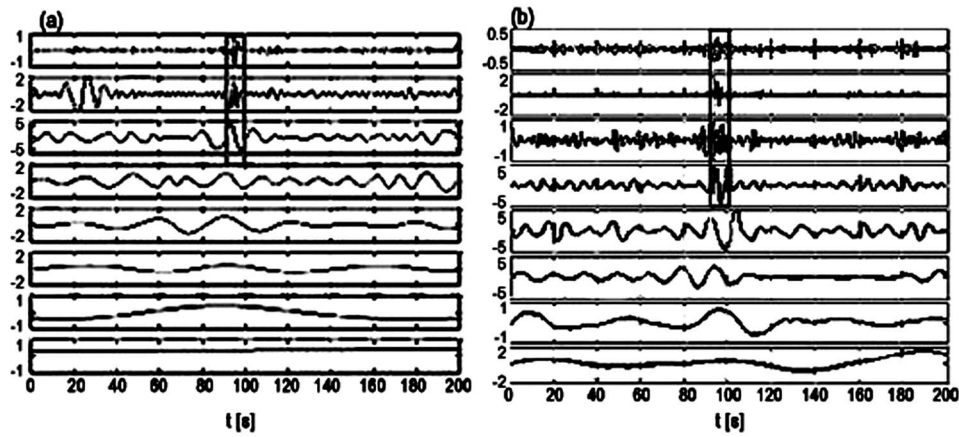


Fig. 12. (a) IMFs of measured transient wave (IMFs 1–8 from top to bottom) and (b) discrete wavelet decomposition of measured transient wave (details 1–8 from top to bottom). Box indicates range of components contributing to sudden amplitude increase

with a dramatic spread in energy, characteristic of sudden discontinuities. This is accompanied by a superposition of the wavelet instantaneous power spectra at each moment in time [Fig. 11(d)], demonstrating the resolution capabilities of wavelets, identifying the dominant carrier wave, as well as a secondary wave component. A clearer perspective of the wavelet representation is provided by the WIFS in Fig. 11(e), which characterizes the transient wave as the combination of two dominant wave components—coalescing near 100 s—to yield a dramatic increase in amplitude. This is in sharp contrast to the EMD+HT spectral representation in Fig. 11(f), which yields a rich display of energy over a wide range of frequencies, including a more abrupt frequency variation near 100 s. Note that the IMFs contributing to this spectrum were obtained by EMD with the following conditions: The maximum iteration number for each sifting was chosen as 1,000. The number of successive sifting steps—that produce

the same number of extrema and zero crossings—was limited to 5. Other sifting criteria may yield some variations in the IMFs obtained.

It is of particular interest to identify the physical mechanisms that enable the formation of the transient wave in Fig. 11(a). Through an inspection of the IMFs in Fig. 12(a), it is evident that the large amplitude component is comprised of energy at a number of scales. Schlurmann (2000) identifies this as a superposition of “selected ‘characteristic embedded modes,’ which coincide in phase at the concentration point...” The details of a discrete wavelet transform using the Daubechies (db5) wavelet (Daubechies 1988) are provided in Fig. 12(b), again demonstrating the contributions to this transient arising from waves of different scales in phase with one another, though the dominant contribution is carried in the third IMF or fourth wavelet detail. Inspection of the instantaneous power spectra at specific time

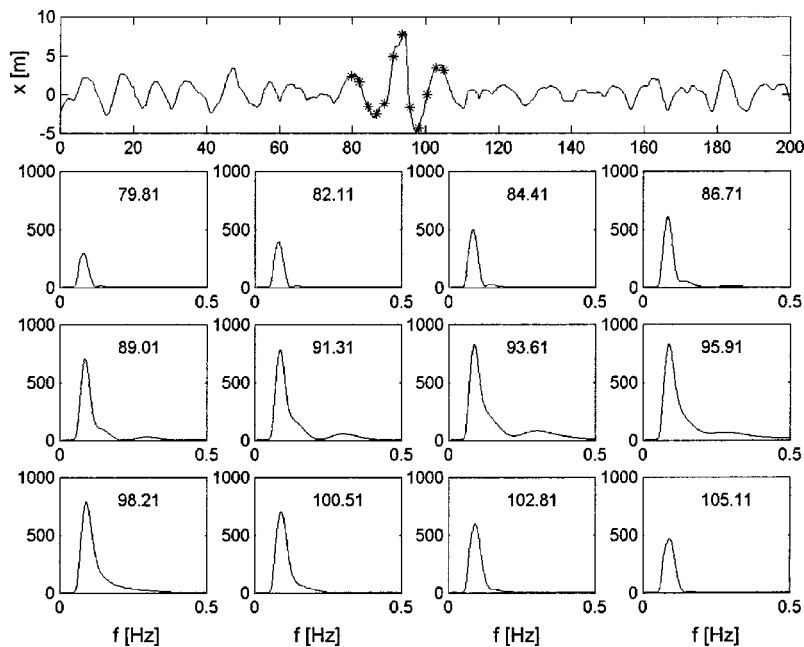


Fig. 13. Measured transient wave and wavelet instantaneous power spectra at times demarcated by asterisks. Time (s) associated with each spectra provided as inset

intervals in the continuous wavelet transform can provide an alternate perspective on such intermittent phenomena (Kijewski et al. 2003). As shown in Fig. 13, these spectra demonstrate that the high amplitude transient wave is the result of the single carrier wave coalescing with higher-frequency waves, leading to a broadened back side spectrum and the presence of a secondary mode at the highest amplitudes of the transient. As the neighboring high-frequency waves move out of phase with the carrier, the spectrum returns to a more symmetric narrowband form, with the amplitudes of the wave diminishing.

Which technique then provides a more faithful representation of the physical phenomenon? Both the discrete wavelet transform and EMD present a fairly consistent decomposition of phase-aligned multiscale contributions to the transient wave; however, the Hilbert transform IF estimate from those IMFs produces a wide spectrum of energetic components, despite the regularity of the waveform. It is unclear whether any physical justification can be inferred for the wide array of components in Fig. 11(f), or if they are attributed to the high variability of IF estimated from the phase (Feldman and Braun 1995). On the other hand, the wavelet representation shows a gradual modulation of frequency—with an intensification of amplitude—at the time of the transient, and the presence of coalescing of waves at multiple scales. The wavelet concept of fitting local harmonics provides an explanation for this smoothed representation.

Conclusions

This study revisited many of the continuous wavelet examples used to establish the efficacy of the EMD+HT, not to advocate for the use of one over the other, but rather to dispel some of the misconceptions surrounding these results. While the examples provided herein have reassessed the performance of the wavelet transform and EMD+HT for a number of nonlinear and nonstationary systems, these results are not achieved without a proper understanding of each approach. Huang et al. (1998) and Dätig and Schlurmann (2004) go to great lengths to explain nuances of the sifting and spline fitting of EMD, as well as extensions of IMFs by characteristic waves to minimize end effects. By the same token, the users of continuous wavelet transforms must be cognizant that the result of their analysis relies heavily on the parent wavelet employed, the discretization of scales, and treatment of end effects (Kijewski-Correa 2003). Specifically, when using the Morlet wavelet, users should make careful selections of the central frequency (Kijewski and Kareem 2003) to completely exploit the resolution capabilities. Improper temporal resolution of the wavelet is shown (see Stokes wave example) to produce results that approach a traditional Fourier analysis, while refined temporal resolutions are capable of identifying nonlinear and nonstationary signal characteristics. Such a lack of understanding of either transform or misrepresentative comparisons of EMD+HT results to scalograms, as opposed to the WIFS, will yield the misleading results often reported in the literature.

While the physical meaning of the EMD+HT result was questioned in two examples involving closely spaced cosine waves and an amplitude-modulated constant frequency oscillator, the two approaches provided comparable evidence of nonstationary and nonlinear behavior for a number of other examples. However, this evidence was presented in distinctly different manners: The IF of the HT detects both subcyclic and supercyclic frequency modulations: The wavelet IF, on the other hand, generally detects supercyclic frequency characteristics and relies

on the instantaneous bandwidth to provide additional subcyclic information. This finding is expected, as the continuous Morlet wavelet fits small waves over a local window in time. As such, the IF corresponds to the sine producing the best local fit to the data. However, this analysis is a local summation of dilated wavelets and, therefore, additional neighboring scales may be required to faithfully represent the data. Meaningful information on the spread of frequencies about this mean or best-fit IF is carried in the instantaneous bandwidth measure, serving as the key to uncovering subcyclic or intrawave phenomena. Given that both transforms can represent nonlinear characteristics, albeit differently, the selection of one approach over the other is entirely dependent on the perspective desired.

Acknowledgments

The writers gratefully acknowledge support, in part, from the NSF (Grant No. CMS 00-85109) and the Center for Applied Mathematics at the University of Notre Dame. The writers are thankful to Professor John M. Niedzwecki for providing the wave tank data. Finally, the assistance of Ms. Lijuan Wang, of the University of Notre Dame, in processing of the freak wave data is gratefully acknowledged.

References

- Boashash, B. (1992a). "Estimating and interpreting the instantaneous frequency of a signal. Part II: Algorithms and applications." *Proc. IEEE*, 80(4), 540–568.
- Boashash, B. (1992b). "Estimating and interpreting the instantaneous frequency of a signal. Part I. Fundamentals and applications." *Proc. IEEE*, 80(4), 520–538.
- Carmona, R. A., Hwang, W. L., and Torresani, B. (1998). *Wavelet analysis and applications: Practical time-frequency analysis*, Academic, San Diego.
- Dätig, M., and Schlurmann, T. (2004). "Performance and limitations of Hilbert-Huang transformation (HHT) with an application to irregular water waves." *Ocean Eng.*, 31(15), 1783–1834.
- Daubechies, I. (1988). "Orthonormal bases and compactly supported wavelets." *Commun. Pure Appl. Math.*, 41, 909–996.
- Delprat, N., et al. (1992). "Asymptotic wavelet and Gabor analysis: Extraction of instantaneous frequencies." *IEEE Trans. Inf. Theory*, 38(2), 644–664.
- Feldman, M. (1994). "Nonlinear system vibration analysis using Hilbert transform. I. Free vibration analysis method 'FREEVIB'." *Mech. Syst. Signal Process.*, 8(2), 119–127.
- Feldman, M., and Braun, S. (1995). "Identification of nonlinear system parameters via the instantaneous frequency: Application of the Hilbert transform and Wigner-Ville techniques." *Proc., 13th International Modal Analysis Conference*, SPIE, Bellingham, WA, 637–642.
- Gabor, D. (1946). "Theory of communication." *Proc. IEEE*, 93(III), 429–457.
- Grossman, A., and Morlet, J. (1985). "Decompositions of functions into wavelets of constant shape and related transforms." *Mathematics and physics, lecture on recent results*, L. Streit, ed., World Scientific, Singapore, 135–165.
- Gurley, K., and Kareem, A. (1999). "Applications of wavelet transforms in earthquake, wind, and ocean engineering." *Eng. Struct.*, 21, 149–167.
- Huang, N. E. et al. (2003). "A confidence limit for the empirical mode decomposition and Hilbert spectral analysis." *Proc. R. Soc. London*, 459, 2317–2345.
- Huang, N. E. et al. (1998). "The empirical mode decomposition and

- the Hilbert spectrum for nonlinear and nonstationary time series analysis." *Proc. R. Soc. London, Ser. A*, 454, 903–995.
- Kareem, A., and Kijewski, T. (2002). "Time-frequency analysis of wind effects on structures." *J. Wind. Eng. Ind. Aerodyn.*, 90, 1435–1452.
- Kijewski, T., Brown, D., and Kareem, A. (2003). "Identification of dynamic properties of a tall building from full-scale response measurements." *Proc., 11th International Conference on Wind Engineering* (CD-ROM), Texas Tech Univ., Lubbock, Tex.
- Kijewski, T., and Kareem, A. (2002). "Wavelet transforms for system identification and associated processing concerns." *Proc., 15th Engineering Mechanics Conference* (CD-ROM), ASCE, Reston, Va.
- Kijewski, T., and Kareem, A. (2003). "Wavelet transforms for system identification in civil engineering." *Comput. Aided Civ. Infrastruct. Eng.*, 18(5), 341–357.
- Kijewski-Correa, T. (2003). *Full-scale measurements and system identification: A time-frequency perspective*, Ph.D. thesis, Univ. of Notre Dame, Notre Dame, Ind.
- Lee, J. K., and Park, Y. S. (1994). "The complex envelope signal and an application to structural modal parameter estimation." *Mech. Syst. Signal Process.*, 8, 129–144.
- Mallat, S. (1998). *A wavelet tour of signal processing*, Academic, San Diego.
- Olhede, S., and Walden, A. T. (2004). "The Hilbert spectrum via wavelet projections." *Proc. R. Soc. London, Ser. A*, 460, 955–975.
- Priestley, M. B. (1988). *Nonlinear and nonstationary time-series analysis*, Academic, San Diego.
- Rihaczek, A. (1966). "Hilbert transforms and the complex representation of signals." *Proc. IEEE*, 54, 434–435.
- Schlurmann, T. (2002). "Spectral analysis of nonlinear water waves based on the Hilbert-Huang transformation." *ASME J. Offshore Mech. Arct. Eng.*, 124(2), 22–27.
- Staszewski, W. J. (1998). "Identification of nonlinear systems using multiscale ridges and skeletons of the wavelet transform." *J. Sound Vib.*, 214(4), 639–658.
- Ville, J. (1948). "Theorie et application de la notion de signal analytical." *Cables Transm.*, 2A(1), 61–74.
- Wu, Z., and Huang, N. E. (2004). "A study of the characteristic of white noise using the empirical mode decomposition method." *Proc. R. Soc. London, Ser. A*, 460, 1597–1611.